

Supplementary Materials
Molecular Biology of the Cell
Bailey *et al.*

Supplemental Information

Loops and the activity of loop extrusion factors constrain chromatin dynamics

Mary Lou P. Bailey^{1,2*}, Ivan Surovtsev^{3,4**}, Jessica F. Williams^{4*}, Hao Yan^{2,3*}, Tianyu Yuan^{2,3}, Kevin Li⁴, Katherine Duseau⁴, Simon G. J. Mochrie^{1,2,3#} and Megan C. King^{2,4,5#}

¹ *Department of Applied Physics, Yale University, New Haven, Connecticut 06511, USA*

² *Integrated Graduate Program in Physics Engineering Biology, Yale University, New Haven, Connecticut 06511, USA*

³ *Department of Physics, Yale University, New Haven, Connecticut 06511, USA*

⁴ *Department of Cell Biology, Yale School of Medicine, New Haven, Connecticut 06520, USA*

⁵ *Department of Molecular, Cell and Developmental Biology, Yale University, New Haven, Connecticut 06511, USA*

* equal contributions

correspondence to simon.mochrie@yale.edu, megan.king@yale.edu, or ivan.surovtsev@yale.edu

Table of contents:

Supplemental Figures S1-S5	2
Supplemental Table S1: MSD Fitting Results	6
Supplemental Table S2: Loop-extrusion-factor (LEF) Simulation and Rouse Simulation Parameters	7
Supplemental Table S3: Strains used in the study	8

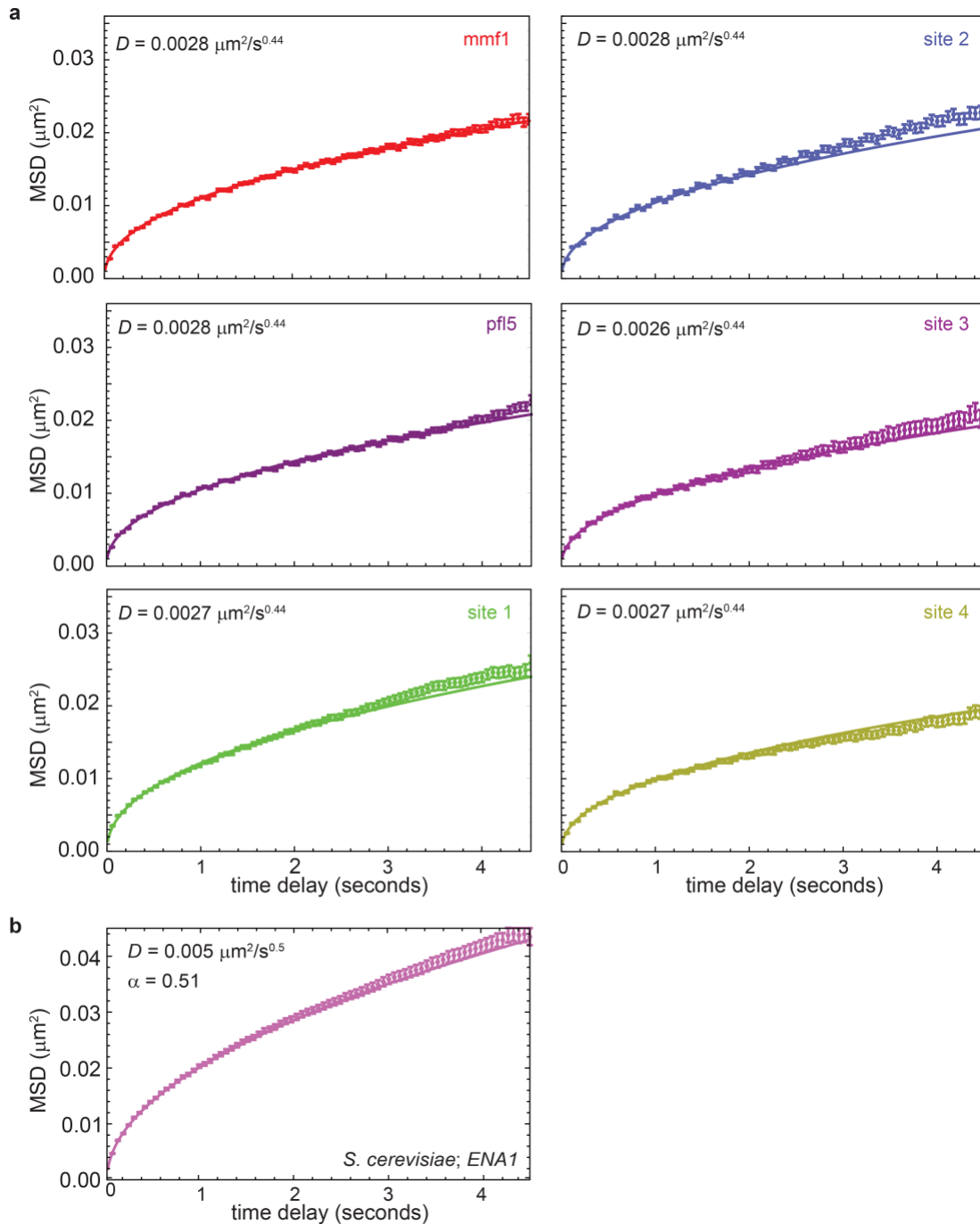


Fig. S1. Individual MSD plots for fission yeast and budding yeast. (a) Chromatin diffusivity is nearly identical across six different genomic locations as shown by the mean squared displacement (MSD) of each genetic locus as a function of the time window of observation, along with its calculated diffusion coefficient, D . **(b)** For comparison to previous chromatin dynamics measurements, we performed our visualization/tracking/diffusive analysis regime on *S. cerevisiae* cells integrated with a *lacO* array at the *ENA1* locus, resulting in a comparable diffusion coefficient as reported previously. Error bars indicate standard errors of the mean.

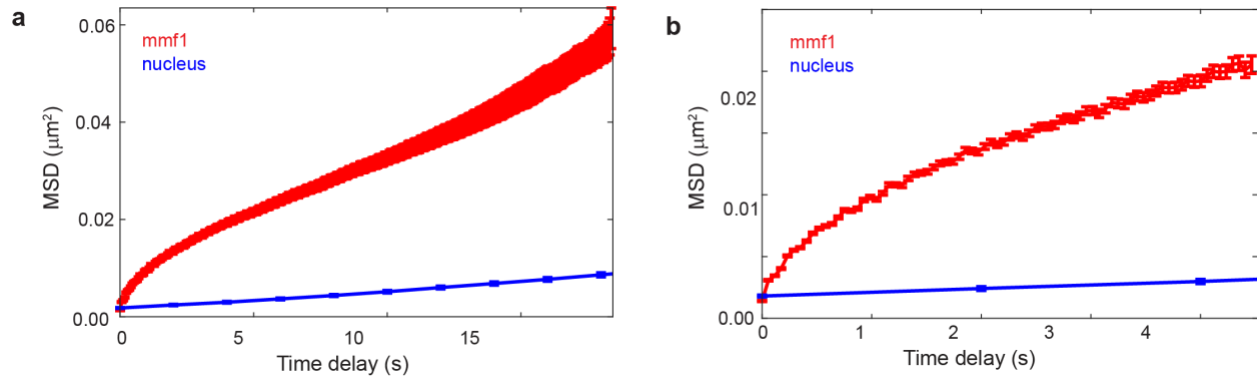


Fig. S2. Microtubule dynamics-driven chromatin motion cannot be explained by whole-nucleus motion. (a) and **(b)** MSD of *lacO* array near *mmf1* relative to MSD of the whole-nucleus motion at different timescales.

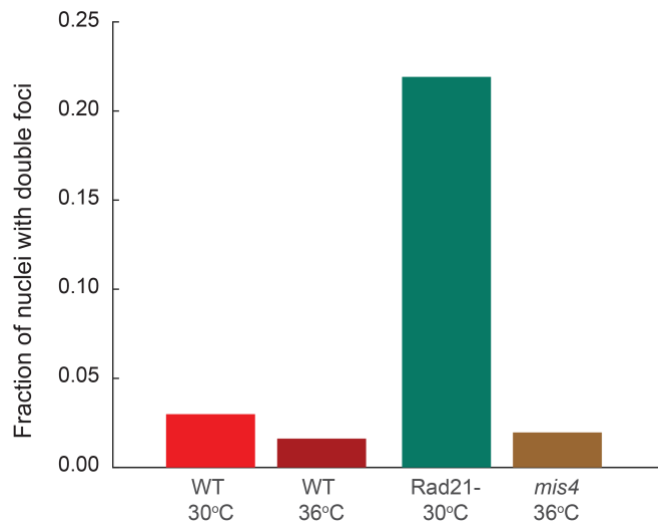


Fig. S3. Cohesin depletion but not inactivation of cohesin loading leads to loss of cohesion. Shown is a fraction of nuclei (of all nuclei with spots) with two spatially separated *lacO*/GFP-LacI foci as observed in single-plane time-lapse movies (details are in the Materials and Methods) for cells with *lacO* array near *mmf1* locus in wild type cells (MKSP2039) at 30C and 36C, and in cells depleted of Rad21 (MKSP3660, at 30C) or with inactivated temperature-sensitive Mis4 (MKSP2801, at 36C).

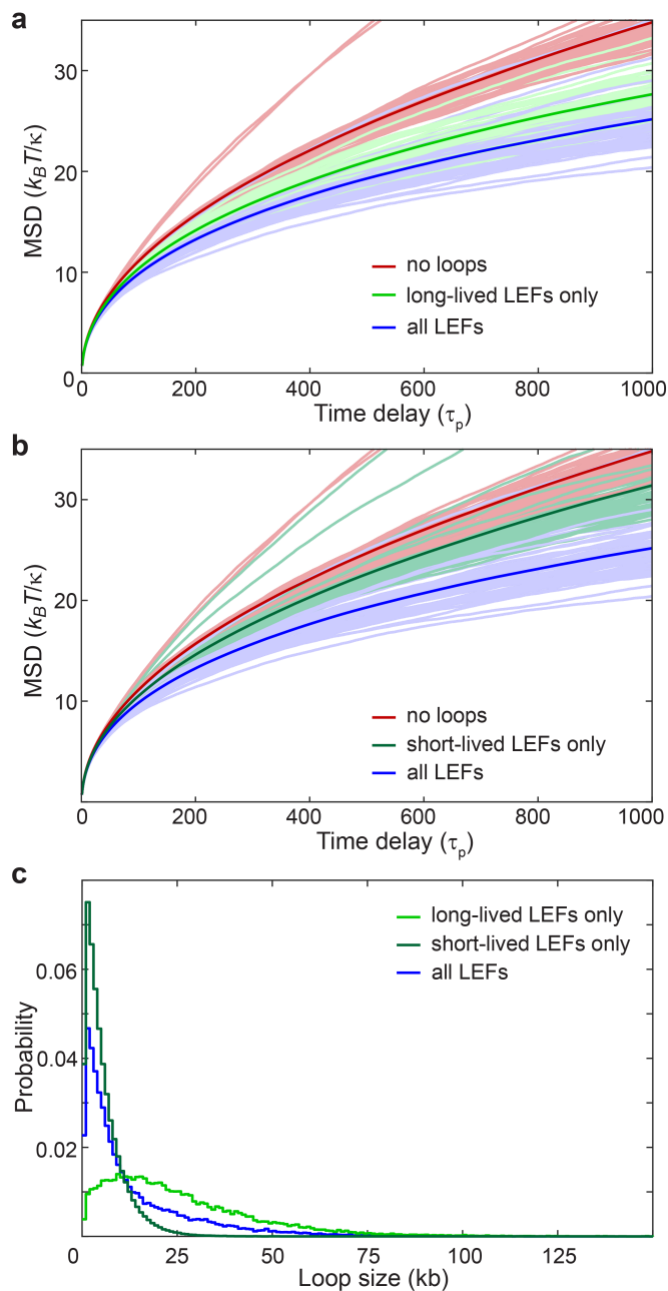


Fig. S4. Impact of LEFs on chromatin mobility depends on LEF lifetime(s). As in Fig. 5a but showing MSDs for individual beads split into two panels for clarity. **(a)** MSD results of the Rouse-type polymer simulations combined with loop-extrusion simulations that considered two types of LEF complexes (in equal amounts) with different lifetimes. Blue – simulations with both types of LEFs present, green – only the long-lived LEFs, red – no LEFs. Thin lines represent MSDs for each individual bead, thick lines represent the average over all beads and all simulations. **(b)** As for (a) but for simulations with only short-lived LEFs (dark green) compared to simulations with both LEFs (blue) and no LEFs (red). **(c)** Loop size distribution for simulations of fission yeast chromatin subjected to the “2 LEFs” model with both LEFs present (blue), only the long-lived LEFs present (green), and only the short-lived LEFs present (dark green).

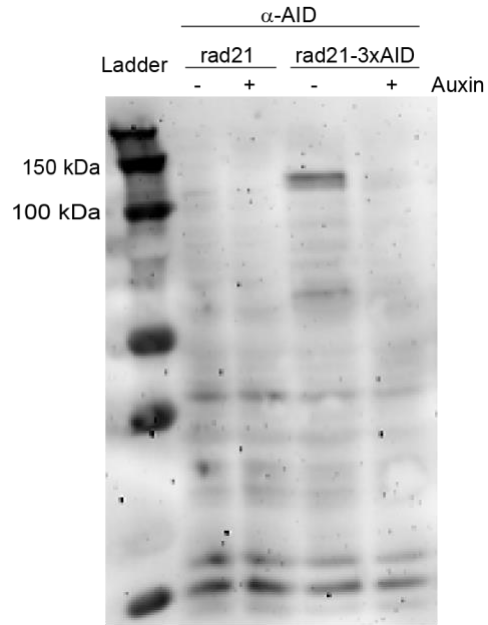


Fig. S5. Rad21-AID can be quickly depleted from cells upon addition of the auxin analogue, 5-IAA. Western blots of lysates of WT cells or cells with Rad21 tagged with auxin-inducible degron before or after 5-IAA treatment for 20 min.

Supplemental Table S1: MSD Fitting Results

Strain	Varied α , σ^2 , D						Fixed $\alpha = 0.44$, varied σ^2 , D				
	α	Confidence Interval (CI) on α fit	σ^2 , μm^2	CI on σ^2 , μm^2	D , $\mu\text{m}^2/\text{s}$	CI on D , $\mu\text{m}^2/\text{s}$	α	σ^2 , μm^2	CI on σ^2 , μm^2	D , $\mu\text{m}^2/\text{s}$	CI on D , $\mu\text{m}^2/\text{s}$
mmf1 WT	0.43	0.3695 - 0.4955	0.0031	0.0027 - 0.0035	0.0028	0.0025 - 0.0032	0.44	0.0031	0.0030 - 0.0032	0.0028	0.0027 - 0.0029
pfl5 WT	0.42	0.3613 - 0.4883	0.003	0.0026 - 0.0034	0.0028	0.0025 - 0.0031	0.44	0.0031	0.0030 - 0.0032	0.0027	0.0026 - 0.0028
site 1	0.53	0.4910 - 0.5776	0.0033	0.0031 - 0.0035	0.0027	0.0025 - 0.0029	0.44	0.0027	0.0026 - 0.0029	0.0031	0.0030 - 0.0031
site2	0.41	0.3092 - 0.5172	0.0032	0.0025 - 0.0039	0.0028	0.0023 - 0.0033	0.44	0.0034	0.0032 - 0.0036	0.0027	0.0026 - 0.0028
site 3	0.43	0.3662 - 0.4901	0.003	0.0026 - 0.0034	0.0026	0.0023 - 0.0028	0.44	0.0031	0.0029 - 0.0032	0.0025	0.0025 - 0.0026
site 4	0.41	0.3540 - 0.4641	0.0028	0.0024 - 0.0031	0.0027	0.0024 - 0.0030	0.44	0.0029	0.0028 - 0.0030	0.0025	0.0025 - 0.0026
mmf1 cut14 36C	0.54	0.5081 - 0.5764	0.0029	0.0027 - 0.0032	0.0032	0.0031 - 0.0034	0.44	0.0022	0.0021 - 0.0023	0.0037	0.0037 - 0.0038
mmf1 mis4 36C	0.47	0.3828 - 0.5503	0.003	0.0023 - 0.0038	0.004	0.0035 - 0.0045	0.44	0.0028	0.0026 - 0.0031	0.0042	0.0040 - 0.0043
pfl5 cut14 36C	0.43	0.3918 - 0.4750	0.0025	0.0022 - 0.0029	0.0035	0.0033 - 0.0038	0.44	0.0026	0.0025 - 0.0027	0.0035	0.0035 - 0.0036
pfl5 mis4 36C	0.44	0.3187 - 0.5572	0.003	0.0019 - 0.0040	0.0039	0.0031 - 0.0047	0.44	0.003	0.0027 - 0.0033	0.0039	0.0037 - 0.0041
mmf1 36C	0.48	0.4462 - 0.5170	0.0031	0.0029 - 0.0033	0.0027	0.0026 - 0.0028	0.44	0.0029	0.0028 - 0.0029	0.0029	0.0028 - 0.0029
pfl5 36C	0.45	0.4154 - 0.4839	0.0026	0.0024 - 0.0028	0.0025	0.0024 - 0.0027	0.44	0.0026	0.0025 - 0.0026	0.0026	0.0026 - 0.0027
mmf1 cut14 rad21- 30C	0.36	0.3292 - 0.3932	0.0026	0.0022 - 0.0029	0.0046	0.0043 - 0.0049	0.44	0.0033	0.0032 - 0.0035	0.0040	0.0039 - 0.0041
mmf1 cut14 rad21- 36C	0.41	0.3750 - 0.4470	0.0028	0.0025 - 0.0032	0.0043	0.004 - 0.0046	0.44	0.0031	0.0031 - 0.0032	0.0041	0.0040 - 0.0041
mmf1 + PFA	near flat MSD	0.0033	0.0029 - 0.0036	5.5×10^{-5}	-2.1×10^{-4} - 3.3×10^{-4}		0.44	0.0033	0.0032 - 0.0034	0.00005	
mmf1 + NaN ₃	0.46	0.3384 - 0.5864	0.0029	0.0025 - 0.0033	0.0014	0.0011 - 0.0017	0.44	0.0028	0.0027 - 0.0029	0.0015	0.0014 - 0.0016
mmf1 + MBC	0.42	0.3327 - 0.4717	0.0027	0.0023 - 0.0032	0.0028	0.0024 - 0.0032	0.44	0.0029	0.0028 - 0.0031	0.0026	0.0026 - 0.0027
cen2 + + MBC	0.55	0.1309 - 0.9721	0.0042	0.0029 - 0.0054	0.0014	6.2×10^{-4} - 0.0023	0.44	0.0038	0.0033 - 0.0043	0.0017	0.0014 - 0.0020
arp8	0.68	0.4822 - 0.8815	0.004	0.0034 - 0.0046	0.0017	0.0014 - 0.0021	0.44	0.0031	0.0027 - 0.0034	0.0024	0.0022 - 0.0025
arp8 cut14 30C	0.54	0.4857 - 0.5969	0.003	0.0028 - 0.0033	0.0021	0.0020 - 0.0023	0.44	0.0026	0.0024 - 0.0027	0.0025	0.0024 - 0.0025
arp8 cut14 36C	0.68	0.6290 - 0.7331	0.0034	0.0032 - 0.0037	0.0023	0.0022 - 0.0024	0.44	0.0023	0.0020 - 0.0025	0.0031	0.0030 - 0.0032
arp9	0.44	0.2652 - 0.6106	0.0037	0.0027 - 0.0047	0.0026	0.0019 - 0.0034	0.44	0.0037	0.0034 - 0.0040	0.0026	0.0025 - 0.0028
<i>S. cerevisiae</i> ENA	0.506	0.48 - 0.5326	0.0033	0.0031 - 0.0036	0.005	0.0048 - 0.0052				0.005	

Supplemental Table S2: Loop-extrusion-factor (LEF) Simulation and Rouse Simulation Parameters

	Mouse CTCF Model	Mouse LEF Only Model	<i>S. pombe</i> LEF Only Model	<i>S. pombe</i> 2 LEFs Model
LEF stepping rate v (bp/s)	60	60	60	60
LEF mean lifetime (s)	2000	2000	500	500, 50
Boundary elements parameter S	20	N/A	N/A	N/A
Boundary elements parameter μ	3	N/A	N/A	N/A
Number of LEFs	48	48	30	15, 15
Polymer characteristic time (s)	0.9	0.9	0.00225	0.00225
Rouse spring stiffness ($\text{pN}\cdot\mu\text{m}^{-1}$)	0.3	0.3	6	6
Friction coefficient ($\text{pN}\cdot\text{s}\cdot\mu\text{m}^{-1}$)	1.08	1.08	0.054	0.054

Supplemental Table S3: Strains used in the study

Strain	Relevant genotype	Description	Source
<i>S. pombe</i>			
Specific lacO position			
MKSP1642	<i>h+ leu1-32 ura4-D18 his7+:P_{Dis1}-gfp-lacI-NLS sad1::sad1-dsRed-leu+ cen2::ura4-lacO_n</i>	WT strain with <i>lacO</i> array integrated near <i>cen2</i> (Chr2 centromere) locus and with expression of LacI-GFP (with nucleus localization signal) under control of the constitutive promoter. Fig. 2.	<i>this study derived from</i> PX342 and PN10127
MKSP1661	<i>h- leu1-32 ura4-D18 his7+:P_{Dis1}-gfp-lacI-NLS cut11::cut11-mCherry-natR pfl5::ura4-lacO_n</i>	WT strain with <i>lacO</i> array (5.6 kb) integrated near <i>pfl5</i> locus (at <i>ChrII</i> : 4403547-4403553). Fig. 1b, 3b, Fig. S1a.	[1]
MKSP1794	<i>leu1-32 ura4-D18 mis4::mis4-242^{ts} his7+:P_{Dis1}-gfp-lacI-NLS cut11::cut11-mCherry-natR pfl5::ura4-lacO_n</i>	Temperature-sensitive mutant of Mis4 cohesin loading factor with <i>lacO</i> array (5.6 kb) integrated near <i>pfl5</i> locus. Fig. 3b.	<i>this study derived from</i> MY3655 and MKSP1340
MKSP2039	<i>h+ leu1-32 ura4-D18 his7+:P_{Dis1}-gfp-lacI-NLS mmf1::ura4-lacO_n</i>	WT strain with <i>lacO</i> array (10.3 kb) integrated near <i>mmf1</i> locus (at <i>ChrII</i> :3442981). Fig. 1b-c, 2, 3a, 5, 7, Fig. S1a, S2	<i>this study derived from</i> MKSP1381
MKSP2583	<i>h- leu1-32 ura4-D18 arp8::hygR his7+:P_{Dis1}-gfp-lacI-NLS mmf1::ura4-lacO_n urg1::loxP-kanR-loxM3</i>	<i>arp8</i> (INO80 complex subunit) deletion mutant with <i>lacO</i> array (10.3 kb) integrated near <i>mmf1</i> locus. Fig. 7.	<i>this study derived from</i> MKSP2190
MKSP2693	<i>leu1-32 ura4-D18 cut14::cut14-208^{ts} cut11::cut11-mCherry-natR his7+:P_{Dis1}-gfp-lacI-NLS pfl5::ura4-lacO_n</i>	Temperature-sensitive mutant of Cut14 condensin subunit with <i>lacO</i> array (5.6 kb) integrated near <i>pfl5</i> locus. Fig. 3b.	<i>this study derived from</i> MY1983
MKSP2760	<i>leu1-32 ura4-D18 cut14::cut14-208^{ts} his7+:P_{Dis1}-gfp-lacI-NLS mmf1::ura4-lacO_n</i>	Temperature-sensitive mutant of Cut14 condensin subunit with <i>lacO</i> array (10.3 kb) integrated near <i>mmf1</i> locus. Fig. 3a, 5b.	<i>this study derived from</i> MY1997
MKSP2801	<i>leu1-32 ura4-D18 mis4::mis4-242^{ts} his7+:P_{Dis1}-gfp-lacI-NLS cut11::cut11-mCherry-natR mmf1::ura4-lacO_n</i>	Temperature-sensitive mutant of Mis4 cohesin loading factor with <i>lacO</i> array (10.3 kb) integrated near <i>mmf1</i> locus. Fig. 3a.	<i>this study derived from</i> MY3655 and MKSP1340
MKSP3021	<i>leu1-32 ura4-D18 arp9::kanR his7+:P_{Dis1}-gfp-lacI-NLS mmf1::ura4-lacO_n</i>	<i>arp9</i> (SWI/RSC complexes subunit) deletion with <i>lacO</i> array (10.3 kb) integrated near <i>mmf1</i> locus. Fig. 7a.	<i>this study derived from</i> MKSP2352
MKSP3053	<i>leu1-32 ura4-D18 arp8::kanR cut14::cut14-208^{ts} his7+:P_{Dis1}-gfp-lacI-NLS mmf1::ura4-lacO_n</i>	Double mutant with <i>arp8</i> deletion and temperature-sensitive mutant of Cut14 condensin subunit with <i>lacO</i> array (10.3 kb) integrated near <i>mmf1</i> locus. Fig. 7b.	<i>this study derived from</i> MKSP2187

MKSP3660	<i>leu1-32</i> <i>cut14::cut14-208^{ts}</i> <i>his7+::P_{Dis1}-gfp-lacI-NLS</i> <i>mmf1::ura4-lacO_n</i> <i>rad21::rad21-XTEN17-3sAID-kanR</i> <i>ura4::ura4-P_{adh1}-OsTir1-F74A</i>	Double mutant bearing temperature-sensitive allele of Cut14 condensin subunit and rad21 cohesin subunit tagged with auxin-inducible degron with <i>lacO</i> array (10.3 kb) integrated near <i>mmf1</i> locus. Fig. 5b	<i>this study derived from</i> DY48569
<i>Random lacO position</i>			
MKSP3117	<i>h+ leu1-32 ura4-D18</i> <i>his7+::P_{Dis1}-gfp-lacI-NLS</i> <i>random locus::ura4-lacO_n</i>	WT strain with <i>lacO</i> array (10.3 kb) integrated at random locus of the genome (noted as “site1”), and with LacI-GFP (with nucleus localization signal) under control of the constitutive promoter. Fig. 1b, Fig. S1a.	<i>derived from</i> MKSP1120
MKSP3118	<i>h+ leu1-32 ura4-D18</i> <i>his7+::P_{Dis1}-gfp-lacI-NLS</i> <i>random locus::ura4-lacO_n</i>	Same as MKSP3117 but with a different random <i>lacO</i> array position (noted as “site2”). Fig. 1b, Fig. S1a.	<i>derived from</i> MKSP1120
MKSP3119	<i>h+ leu1-32 ura4-D18</i> <i>his7+::P_{Dis1}-gfp-lacI-NLS</i> <i>random locus::ura4-lacO_n</i>	Same as MKSP3117 but with a different random <i>lacO</i> array position (noted as “site3”). Fig. 1b, Fig. S1a.	<i>derived from</i> MKSP1120
MKSP3123	<i>h+ leu1-32 ura4-D18</i> <i>his7+::P_{Dis1}-gfp-lacI-NLS</i> <i>random locus::ura4-lacO_n</i>	Same as MKSP3117 but with a different random <i>lacO</i> array position (noted as “site4”). Fig. 1b, Fig. S1a.	<i>derived from</i> MKSP1120
<i>Labeled nuclear envelope strain</i>			
MKSP3140	<i>h+ leu1-32 ura4-D18</i> <i>his7+::P_{Dis1}-gfp-lacI-NLS</i> <i>cut11::cut11-mCherry-natR</i> <i>isd90::ura4-lacO_n</i>	WT strain with <i>lacO</i> array (10 kb) integrated near <i>isd90</i> locus (at <i>ChrII: 1950422</i>). Fig. S2.	
<i>Auxiliary strains</i>			
AW563	<i>h- leu1-32</i> <i>urg1::loxP-kanR-loxM3₆</i>	WT strain with recombination-mediated cassette exchange system (<i>RMCE_{kanMX6}</i>).	[2]
DY48569	<i>h+ mat1PA17</i> <i>leu1-32 lys1-131 ade6-M216</i> <i>ura4::ura4-P_{adh1}-OsTir1-F74A</i>	Strain bearing an auxin-inducible degron system	YGRC FY39923 [3]
JM210 FN198 MKSP1116	<i>h- leu1-32 ura4-D18 ade-</i> <i>cut11::cut11-mCherry-natMX6</i>	WT strain with Cut11-mCherry (a nuclear envelope marker) expression controlled by the native promoter.	<i>Nurse lab</i>
MKSP1120	<i>h+ leu1-32 ura4-D18</i> <i>his7+::P_{Dis1}-gfp-lacI-NLS</i>	WT strain with LacI-GFP (with nucleus localization signal) under control of the constitutive promoter. Used to generate random <i>lacO</i> array integrations.	
MKSP1340	<i>h- leu1-32 ura4-D18</i> <i>his7+::P_{Dis1}-gfp-lacI-NLS</i> <i>cut11::cut11-mCherry-natR</i> <i>mmf1::ura4-lacO_n</i> <i>ChrII:3442981::ura4-lacO_n</i>	WT strain with <i>lacO</i> array (10.3 kb) integrated near <i>mmf1</i> locus and with LacI-GFP (with nucleus localization signal) under control of the constitutive promoter	<i>this study similar to</i> MKSP1381
MKSP1381	<i>h- leu1-32 ura4-D18</i> <i>his7+::P_{Dis1}-gfp-lacI-NLS</i> <i>ChrII:3442981::ura4-10.3kbLacO</i> <i>ChrII:3446249::HOcs-hphMX6</i> <i>cut11::cut11-mCherry-natMX6</i>	Original <i>lacO</i> array (10.3 kb) integration near <i>mmf1</i> locus. Used to generate all other <i>mmf1-lacO_n</i> strains in this study	[4]
MKSP1128	<i>h- leu1-32 ura4-D18</i> <i>his7+::P_{Dis1}-gfp-lacI-NLS</i> <i>cut11::cut11-mCherry-natMX6</i>	WT strain with Cut11-mCherry (a nuclear envelope marker) expression controlled by the native promoter and with LacI-GFP (with nucleus localization signal) under control of the constitutive promoter.	
MKSP2187	<i>h- leu1-32 ura4-D18</i> <i>arp8::kanR</i>	<i>arp8</i> deletion.	<i>this study</i>
MKSP2190	<i>h- leu1-32 ura4-D18</i> <i>arp8::hygR</i>	<i>arp8</i> deletion.	<i>this study</i>

MKSP2352	<i>h- leu1-32 ura4-D18 arp9::kanR</i>	<i>arp9</i> deletion.	<i>this study</i>
MY1983	<i>h- ura4 cut14::cut14-208^{ts}</i>	Strain encoding for the temperature sensitive allele of <i>cut14</i> .	YGRC FY9883
MY1997	<i>h+ cut14::cut14-208^{ts}</i>	Strain encoding for the temperature sensitive allele of <i>cut14</i> .	YGRC FY9897
MY3655	<i>h- leu1-32 mis4::mis4-242^{ts}</i>	Strain encoding for the temperature sensitive allele of <i>mis4</i> .	YGRC FY111578
PN10127	<i>h- sad1::sad1-dsRed-leu+</i>	WT strain with Sad1-dsRed (a spindle pole body marker) expression controlled by the native promoter.	
PX342	<i>h+ leu1-32 ade6-M216 bub1::ura4 cen2-lacO_n</i>	Strain with <i>cen2</i> locus (centromere of ChrII) containing <i>lacO</i> array insertion.	YGRC FY13812 [5]
<i>S. cerevisiae</i>			
PCCPL645	W303 <i>LacI-GFP::HIS</i>	W303 strain with <i>LacI-GFP</i> (with nucleus localization signal) under control of the constitutive promoter.	[6]
PCCPL835	W303 <i>LacI-GFP::HIS ENA-lacO_n::TRP1</i>	W303 strain with <i>lacO</i> array integrated near <i>ENA</i> locus and with <i>LacI-GFP</i> (with nucleus localization signal) under control of the constitutive promoter. <i>Fig. S1b</i> .	<i>this study derived from PCCPL 645 as described [6] and [7]</i>

Table S3 References:

1. Zhao Y., Schreiner S.M., Koo P.K., Colombi P., King M.C., Mochrie S.G. (2016) Improved Determination of Subnuclear Position Enabled by Three-Dimensional Membrane Reconstruction. ***Biophys. J.*** 111, 19-24.
2. Watson A.T., Werler P., Carr A.M. (2011) Regulation of gene expression at the fission yeast *Schizosaccharomyces pombe* *urg1* locus. ***Gene*** 484, 75-85.
3. Zhang X.-R. Zhao L., Suo F., Gao Y., Wu Q., Qi X., Du L.-L. (2022) An improved auxin-inducible degron system for fission yeast. ***G3***, 12, jkab393.
3. Leland B.A., Chen A.C., Zhao A.Y., Wharton R.C., King M.C. (2018) Rev7 and 53BP1/Crb2 prevent RecQ helicase-dependent hyper-resection of DNA double-strand breaks. ***eLife*** 7, e33402.
4. Hauf S., Biswas A., Langegger M., Kawashima S.A., Tsukahara T, Watanabe Y. (2007) Aurora controls sister kinetochore mono-orientation and homolog bi-orientation in meiosis-I. ***EMBO J.*** 26, 4475-86.
5. Colombi P., King D.E., Williams J.F., Lusk C.L., King M.C. (2018) LEM domain proteins control the efficiency of adaptation through copy number variation. ***Biorxiv*** 451583, <https://www.biorxiv.org/content/biorxiv/early/2018/10/24/451583.full.pdf>
6. Murray J., Watson A., Carr A. (2016) *Identifying products of recombinase-mediated cassette exchange (RMCE) in Schizosaccharomyces pombe*. **Cold Spring Harbor Protocols**, 2016 (5)